

# A Review on Machine Learning Algorithms for Dust Aerosol Detection using Satellite Data

Nurul Rafi<sup>1</sup> and Pablo Rivas<sup>2</sup> 

School of Engineering and Computer Science  
Department of Computer Science  
Baylor University, Texas, USA

<sup>1</sup>Nurul.Rafi1@Baylor.edu <sup>2</sup>Pablo.Rivas@Baylor.edu

**Abstract.** Dust storms are associated with certain respiratory illnesses across different areas in the world. Researchers have devoted time and resources to study the elements surrounding dust storm phenomena. This paper reviews the efforts of those who have investigated dust aerosols using sensors onboard of satellites using machine learning-based approaches. We have reviewed the most common issues revolving dust aerosol modeling using different datasets and different sensors from a historical perspective. Our findings suggest that multi-spectral approaches based on linear and non-linear combinations of spectral bands are some of the most successful for visualization and quantitative analysis; however, when researchers have leveraged machine learning, performance has been improved and new opportunities to solve unique problems arise.

## 1 Introduction

Dust is the most common form of aerosol globally, affecting the water cycle, plants, public health and welfare, and climate [41]. It is generated at a micro-scale and can affect a wide area depending on wind flow and geomorphology [10]. Dust aerosols are non-spherical airborne particles with depolarization and can be found in large numbers, particularly in areas like Africa's northwestern region. However, researchers discovered that dust aerosols could be found around different continents, regardless of their source [51].

According to some reports, dust aerosol causes extreme air pollution, and a variety of respiratory diseases [53,55]. Dust storms, which contain toxic airborne particles such as organic contaminants, trace products, and cancer-causing bacteria, are deadly weather phenomena that mostly occur in deserts and bare land areas [60,2,19,26]. Dust storms directly impact the global environment by absorbing solar radiation and reducing visual acuity, resulting in dangerous traffic accidents [9,5]. To assess the level of activity of dust storms, researchers evaluate changes in different criteria, including dust day's frequencies [58,17], optical depth index of aerosols [11], and index of a dust storm [42,16], among others [35]. While some of these dust events are evidently visible, as shown in Figure 1, low concentrations of dust at different altitudes can present challenges that

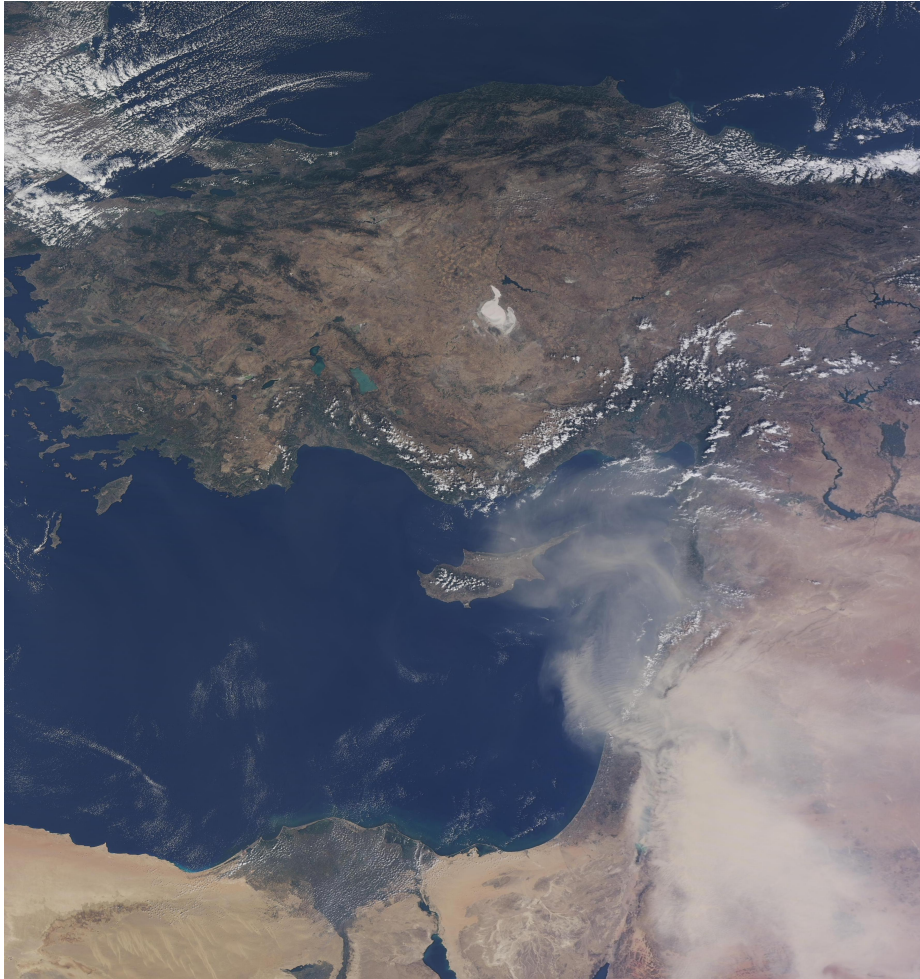


**Fig. 1.** Dust event captured with the MODIS instrument over NASA’s Terra Satellite. Source: West Africa.

require leveraging machine learning methodologies for better results. This paper performs a succinct literature review of machine learning methodologies applied in dust aerosol modeling problems.

This paper is organized as follows: Section 2 introduces the concept of remote sensing for dust aerosols, including the different satellites and sensors commonly used. Section 3 describes data availability and accessibility-related issues. Section 4 presents approaches based on the physical properties of dust, paving the way to understand the feature space of machine learning methodologies, which are discussed in Section 5. Section 6 provides additional information on methods related to dust modeling, and finally, conclusions are drawn in Section 7.

## 2 Remote Sensing for Dust Aerosols

The use of remote sensing (RS) to detect dust sources at both local and regional scales is a valuable tool [7]. Due to the high variability in spatial data, RS has become the standard method for determining the presence and movement of dust aerosols. In addition to AERONET [27] and lidar systems [56], specific RS may be useful depending on the target’s characteristics and location [6]. The majority of satellites are polar orbiting, with higher spectral resolution and a wider range, while geostationary satellites, with their high temporal resolution [60], are used to monitor the formation and growth of dust storms. Geostationary satellites have more channels and resolution for collecting dust temporal variations [31].

### 2.1 Aqua and Terra: MODIS

Four indicators from Moderate Resolution Imaging Spectroradiometer (MODIS) satellite images from both Terra and Aqua satellites [53] have been used in the study of RS around the world to identify dust sources, including Brightness Temperature Differences (band 29–band 31) and (band 31–band 32), as well as the Normalized Difference Dust Index (NDDI) and D variable using Over-land [39,10]. To better understand dust storms, some researchers use MODIS Terra Level 1B radiances to capture images near real-time with 1km resolution. Some models, on the other hand, use the MODIS Aerosol Optical Thickness (AOT) product, which has a 10km resolution and takes several hours to process after obtaining images [50]. The concentration of the AOD product is high, but the spatial resolution is poor [57]. MODIS AOT also ignores fine dust and does not operate in heavy icy clouds [74]. NASA’s EOS (LANCE) offers data almost in real time [51], and is stacked in this website where anybody can search and collect data, with data from MODIS being called a granule every 5 minutes [62].

MODIS data is divided into three levels: Level-0, 1A, and 1B, with Level-1B containing corrected multi-spectral data [54]. The 16 bit thermal emitting bands in 1B level data should be processed to this  $Wm^{-2}\mu m^{-1}sr^{-1}$  unit [28]. With this 3 level info, MODIS provides 36 spectral bands with a spatial resolution of 250m(1-2), 500m(3-7), 1km(8-36) bands [60] and a wavelength range of 0.045 to  $14.385\mu m$  and an instrument angle of 110 degree [6]. Raw telemetry data can be found on Level 0 and raw spectral bands data can be found on Level 1A [54]. For RGB mapping, the bands 1, 4 and 3 are used [49].

### 2.2 CALIPSO

Cloud–Aerosol Lidar and Infrared Pathfinder Satellite Observation (CALIPSO) has a dust dataset with a high frequency. Using its vertical profile [31] and a polar orbiting satellite with a 16-day recycle period [63] and a 5-kilometer range, it can provide more detailed dust information. Dust storms were collected using CALIPSO [23]. CALIPSO can detect vertical distribution in normal time [6]. Though CALIPSO is better at detecting dust, it only collects data from a smaller

area of the Earth's surface [62]. Aside from that, it has a high consuming power and a small coverage field [61].

CALIPSO uses a  $98^\circ$ -inclination orbit to test lidar signals in the  $532$  and  $1064$   $nm$  bands [62] and flies at an altitude of  $705$  km to provide vertical distribution of aerosols and cloud [6]. Based on the probability density function, [33] used CALIPSO data to describe the dust aerosol.

### 2.3 VIRRS

At night, the Visible Infrared Imaging Radiometer Suite loses its solar reflective bands and has 22 channels with wavelengths ranging from  $0.41\mu m$  to  $12.01\mu m$  [30]. 16 have moderate resolution imagery bands, 5 have high resolution imagery bands, and one is a panchromatic day/night band.

### 2.4 CALIOP

The Cloud-Aerosol Lidar with Orthogonal Polarization is a lidar device in space that can measure depolarization and color ratio [35]. At  $532nm$  and  $1064nm$ , CALIOP offers backscatter profiles as well as two orthogonal (parallel and perpendicular) polarization components at  $532nm$  [6]. With the aid of other radiation models, CALIOP data can be useful in achieving radiative and heating rates [22]. Versions 3.01 and 3.02 of the CALIOP Level 2-5 km Aerosol/Cloud layer were used in this paper[63].

### 2.5 MERIS

Dust samples from sand regions were collected using Medium Resolution Imaging Spectrometer (MERIS) [70,12]. Ocean color is also collected by MERIS.

### 2.6 AVHRR

The AVHRR bands 4 and 5 are the same as MODIS 31 and 32 [55]. The NOAA-AVHRR satellites' GAC (Global Area Coverage) data set is an excellent resource for researching in surface conditions caused in part by climatic variation. AVHRR has 5 spectral bands varying from  $0.58 - 12\mu m$  [20].

### 2.7 OMI

Researchers used the OMAERUV product from the Ozone Monitoring Instrument (OMI) sensor to verify the accuracy, as they used the AQUA satellite where OMI is appropriate [65]. It has a high spatial resolution and is used to detect both sources and plumes [6].

### 3 Data Sources and Computer Processing

#### 3.1 Data Collection

Dusty days are described as days with a visibility of less than 2000 meters per hour during the day, as measured by Terra-MODIS images [10,47,46,67]. Terra-MODIS can only generate 23 images per day due to its daily visit to a predetermined location [10]. The MODIS sensor from Terra and Aqua is used for a variety of purposes, including (i) wide angle and high temporal resolution of images (ii) high spatial resolution with various band ranges (iii) a wide variety of spectral bands and ranges [18,36,68,21].

Authors used webscraping to gather data from NASA at various resolutions and times [51]. Researchers used smaller feature vectors with KLT due to high computational complexity and hardware dependence. In order to take at least 30 times training samples of the feature bands, they chose 240 feature vectors based on these two groups. [38,49]. They implemented Balanced Error Rate (BER) as a method of mitigating error to eliminate false positive counts. Bias correction can be used to eliminate inconsistencies in results [25].

#### 3.2 Data Access

Table 1 contains relevant information for accessing data from NASA information systems.

MODIS contains hdf5 files where all the information of the bands are stacked in this format. We have used the file `MOD021KM.A2021092.0020.006.2021092134055.hdf` for data processing and for band information. This is 1km spectral resolution file as the prefix of the file name defines it. In Figure 2, only band 3 is shown in a magma color map using the Python language. For processing hdf5 file and band information Satpy Python package was used.

## 4 Physical approaches

#### 4.1 MODIS Index

They introduced Brightness Temperature Difference for dust detection in this paper [1]. Positive BTM at a high level indicates dense dust, while positive BTM at a low level may also indicate dense dust [65].  $BTM_{3-11}$  is sensitive to dust loading, while  $BTM_{8-11}$  and  $BTM_{11-12}$  will distinguish the dust when used together [31].

$$\begin{aligned} BTM_{11-12} &= BT_{\sim 11.2} - BT_{\sim 12.4} \\ BTM_{3-11} &= BT_{\sim 3.9} - BT_{\sim 11.2} \\ BTM_{8-11} &= BT_{\sim 8.6} - BT_{\sim 11.2} \end{aligned} \tag{1}$$

In the Saharan zone, researchers developed TDI to detect dust [23]. They observed dust storms using NDDI indexing from MODIS data, and four bands

**Table 1.** Data Sources by NASA

Source	URL	Description
LAADS DAAC Level-1 and Atmosphere Archive & Distribution System Distributed Active Archive Center	<a href="https://ladsweb.modaps.eosdis.nasa.gov">https://ladsweb.modaps.eosdis.nasa.gov</a>	MODIS, VIIRS, MERIS, SLSTR, and OLCI are all described in detail.
Terra and Aqua	<a href="https://ladsweb.modaps.eosdis.nasa.gov/missions-and-measurements/modis/">https://ladsweb.modaps.eosdis.nasa.gov/missions-and-measurements/modis/</a>	Terra and Aqua are described in detail, with all technical requirements and channels containing all band information.
VIIRS - Visible Infrared Imaging Radiometer Suite	<a href="https://ladsweb.modaps.eosdis.nasa.gov/missions-and-measurements/viirs/">https://ladsweb.modaps.eosdis.nasa.gov/missions-and-measurements/viirs/</a>	All technical requirements and channels for VIIRS are listed, as well as all band details.
MODIS Level 0-1	<a href="https://ladsweb.modaps.eosdis.nasa.gov/missions-and-measurements/science-domain/modis-L0L1/">https://ladsweb.modaps.eosdis.nasa.gov/missions-and-measurements/science-domain/modis-L0L1/</a>	Both levels of data are accessible in this link's data repository. A total of 8 Terra and Aqua products, as well as MODIS Level 1B calibrated data with spatial resolutions of 250m, 500m, and 1km, are available here.

were used. Dust was separated from water, clouds, and snow using various thresholds [71].

$$NDDI = \frac{B7 - B3}{B7 + B3} \quad (2)$$

NDDI is commonly used in conjunction with BTD because it cannot detect dust on its own [31]. For measuring dust events, various types of indices are used, and multiple indices can be combined to resolve drawbacks and perform better [60]. The BADI and BTR methods eliminate some of the drawbacks of the BTB method [60]. Since it only uses the thermal wavelength, TDI can be used at night as well as during the day while it is over the ocean [31]

$$TDI = C_0 + C_1 \times BT_{3.7} + C_2 \times BT_{9.7} + C_3 \times BT_{11} + C_4 \times BT_{12} \quad (3)$$

BADI is more effective at catching the size and density of dust [31].

$$BADI = \frac{2}{\pi} \times \arctan \left( \frac{BDI}{BDI_{0.95}} \right), \quad (4)$$

$$\text{where } BDI = (BTD_{3.9-11.2})^2 \times BTD_{12.4-11.2}. \quad (5)$$

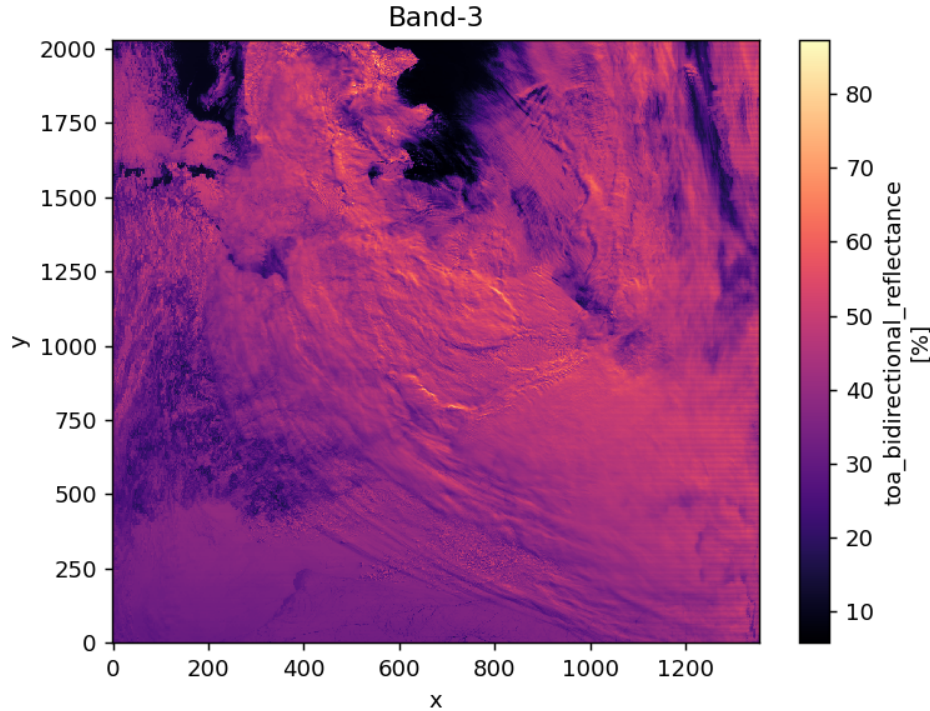


**Fig. 2.** Band-3 in magma color map

## 4.2 Generic

Low level visual grammar scheme describes high level spatial feature [3]. The majority of them avoided feature engineering [62].

# 5 Machine Learning Algorithms

## 5.1 Support Vector-Based

SVM needs a lot of memory and can struggle with large datasets [62]. SVM maximizes the decision boundary of two groups and embraces non-linear classification, but it takes more time to process, which is inconvenient for large datasets [60]. SVM attempts to find the optimal hyperplane [40] by converting non linear problems to linearly separable problems using kernel functions [72]. On their dataset, the authors claimed a precision of up to 98 percent [52]. They used four bands, B20, B29, B31, and B32, and tried to reduce the support vectors to improve the dust event likelihood.

They used TrAdaBoost for SVM transfer learning above 3km altitude with high classification accuracy [35]. SVM for Regression was used to detect dust aerosols in near real time, with the researchers attempting to reduce the time

complexity by minimizing the support vectors [52]. Among the other approaches, Large Scale Linear Programming-SVR performed better in classifier efficiency. The rank of the classifiers is indicated in parenthesis.

Researchers used updated SVM with MODIS L1 data because threshold-based SVM has some disadvantages in terms of complexity and certainty. They discovered that previous methods had difficulty correctly distinguishing dust on bright surfaces. They used the Radial Basis Function to find the best classification observation (RBF) [60]. Since it is dependent on the input data, bias may affect the model's output [31].

In a classification problem, SVM outperforms ANN because it always finds the global minimum. When the regularization parameter  $C = 100$  and the kernel  $\gamma = 0.008$  are both chosen for classification, RBF is the most efficient kernel. Auxiliary data, such as cloud masking, is not required for SVM. SVM worked well in both land and oceans with low dust density, according to their findings. However, they mistook the majority of cloudy pixels for dust. The precision was calculated using the kappa coefficient. They also claimed that SVM is a sufficient tool for dust detection in multispectral images. SVM had an accuracy of 84 percent with a Kappa coefficient of 0.8091, while MLP had an accuracy of 81 percent with a Kappa coefficient of 0.771 [57].  $C$  and  $\gamma$  are commonly used values of 1 and 0.07, respectively, for dust aerosol detection with SVM and CALIPSO data, while  $C(0.25)$  and  $\gamma(0.0078)$  are used for dust aerosol detection with SVM and CALIPSO data [60,34].

SVM was used to identify the best band combinations, which were B7-B3, B20-B31, and B31-B32 [60]. Although SVM has the advantage of using small samples, 5D PDF performed better after the first day of observation [35]. Also, for high dimension or huge number of data, training SVM is difficult [24].

## 5.2 Neural Networks

**Feed-Forward or Dense** The input, secret, and output layers of an artificial neural network are typically represented by feature vectors. Researches proposed for detecting clouds present in the B3 and B7 bands in order to minimize the high complexity of dust image processing. For the gradient, they used the Scaled Conjugate Gradient Algorithm because it is more efficient. The classifier identified three classes: vegetation, soil, and dust [12]. In their study, they used the R packages Neuralnet and SparkR to perform ANN analysis [61]. The neural network was fed the reflection values of the bands as data [57]. The authors recommend two hidden layers, but the most appropriate number of layers and parameters can be determined through repetition and comparison of the best accuracy [37].

Feed Forward Neural Networks (FFNN) functioned similarly to a traditional neural network, with input and output layers as well as hidden layers. Back propagation and the "Levenberg-Marquardt" algorithm were used by the researchers to update weights and prejudice [49]. The error was calculated using the mean squared error (MSE) where between the layers, there is no cycle or loop. 3 secret layers, each with a batch size of 256 and a total of 2000 epochs [30]. Among the



models that used CALIOP products, FFNN had an accuracy of 84.9 percent [30]. In FFNN, they used sigma as an activation function [50].

The researchers used a two-layer Feed-Forward neural network with 15 secret neurons and three neuron outputs [12]. They simplified the process of choosing statistical datasets and eliminating false positives.

**Convolutional** Convolutional Neural Network (CNN) is more suitable for image processing. CNN applies filters to reduce the dimensionality of images without eliminating essential features [30]. SVM has some limitations due to the high dimensionality or huge amount of samples, while ANN has issues with false positives. For dust detection, a developed Naive Bayesian CNN classification technique is being developed. Because  $PM_{2.5}$  concentration is linked to dust, the CNN method is utilized to forecast  $PM_{2.5}$  value [24]. Although the Softmax classifier is utilized for final layer classification in CNN, it is insufficient for splitting the feature space due to high noise in remote sensing data or huge differences between features [64].

In remote sensing images, CNN outperformed traditional methods. Atrous convolution is used in conjunction with separable convolution because it captures a broader context with its larger view of filters, which may perform better in scene categorization in remote sensing [13]. In order to improve accuracy, they merged CNN and advanced MLP in the classification step [59]. Based on ResNet101, the fast deep perception network (FDPResnet) includes deep CNN and Broad Learning System (BLS) for extracting both deep and shallow aspects of remote sensing images. The proposed method performed well in classification in a shorter time using the NWPU-RESISC45 remote sensing dataset [15]. As attention mechanism identifies the most active region in a remote sensing image for better classification [69] first introduced Attention Recurrent Convolutional Network (ARCNnet).

On six popular remote sensing datasets, they applied a new EfficientNet CNN model based on attention mechanism to the last feature map. EfficientNet CNN outperformed earlier approaches, and they employed the Swish activation function, which is smoother than ReLU and LeakyReLU [4]. [32] applied same model with different training rounds (SMDTR) with CNN which performed better than CNN, CapsNet, SMDTR\_CapsNet. CNN was utilized in conjunction with CapsNet, with CNN converting input images into feature maps and CapsNet performing final classification. This integrated strategy outperformed other current approaches on three popular datasets [73].

**Probabilistic** The Probabilistic Neural Network (PNN) is a neuro-statistical hybrid model [49]. PNN is a semi-supervised network since it does not involve learning but operates under supervision [66,14]. It is employed in the classification of dust events. They used a minimized version of feature bands based on the assumption that training samples should be at least three times the size of feature bands due to the large number of feature vectors [45]. For dimension reduction, Principal Component Analysis (PCA) was used. They also used pixel mapping

to address dust likelihood in areas farther away from the dust storm source [48]. It has four layers: input, pattern, summation, and output, with the summation layer centered on individual pattern layers in different groups [54].

The layer performance of a pattern is determined by [49]

$$\varphi_{jk}(\mathbf{F}) = \frac{1}{(2\pi)^{\frac{d}{2}}\sigma^d} e^{-\frac{1}{2\sigma^2}(\mathbf{F}-v_{jk}^F)^T(\mathbf{F}-v_{jk}^F)}, \quad (6)$$

where  $\sigma$  is the absolute difference between the smallest normal variances [49].

Researchers discovered that the Gaussian distribution better describes the frequency of dust storms using MODIS 1B data. Their probabilistic model was also capable of segmentation using the threshold value. They used the formula below to convert units back to the original unit. [53].

$$\hat{X} = \alpha(\beta - \gamma) \quad (7)$$

Where  $\alpha$  and  $\beta$  represent radiance scales and offsets, respectively, and *gamma* represents scaled data intensities.

PNN outperformed the ML classifier in this study [54]. Multi spectral images can be categorized using a probabilistic density function [50]. Their probability density function was dubbed the "data likelihood" function by them [54].

### 5.3 Ensemble Method

**Random forest** For the first time, researchers used Random Forest (RF) for dust classification, except the cloud mask, which was a source of misclassification in previous approaches [65]. It outperforms SVM, AdaBoost, and ANN as an ensemble system. Also with the thin dusts, RF outperformed and in both water and ground [71] [74]. RF can accommodate a large number of inputs without the use of variables [62]. However, their biggest flaw is that they used manual data to train RF, which should have been automated.

It functions best with high-dimensional data because it works with subsets and also determines the value of features, reducing the difficulty of identifying predictor variables. In this study, 100 max depths and 500 estimators were used [30]. Susceptibility mapping was developed from different dust events for classification, and AOC 90.8 RF was performed [10]. For dust detection, a random forest model utilizing the Advanced Baseline Imager (ABI) achieved an AUC of 0.97 [8].

### 5.4 Clustering

**K nearest neighbours** The main benefit is that data does not have to be linearly separable. Hyperparameters were calculated using 10 nearest neighbors using the Euclidean distance calculation [30]. [43] used a k-NN classifier to identify dust in museum locations. The size and shape of the particles are determined using a classification technique where the accuracy is more than 90%.

### 5.5 Maximum Likelihood-Based

Maximum Likelihood Classifier is used for the classification of atmospheric components. It is based on a Bayesian classifier with probabilistic arguments, and two random variables, dust and backgrounds, were chosen [49]. They also counted the two occurrences as having an equal chance of occurring, and then determined the function vector  $F$  that is closest to the classes [49].

$$\psi_{c_i}(x) = (x - \mu_i)^T \Sigma_i^{-1} (x - \mu_i) - \det(\Sigma_i) \quad (8)$$

Where  $\mu_i$  is the mean feature vector and  $\Sigma_i$  is the covariance matrix, and  $\mu$  and  $x$  are derived using ML estimators from training data. The determinant function is "det," and the discriminant function is  $\psi_{c_i}$ , which is quadratic and calculates the distance between  $\mu$  and  $x$  weighted by  $\Sigma_i$ .

Finally, the feature vector will be classified into the two classes that are the most similar. The researchers concluded that the likelihood of dust and background groups was roughly equal. To find the discriminant function and simplify the problem, the log-likelihood of the Gaussian distribution was used. [49]. For satellite image classification, L2 regularization is used with logistic regression [30].

### 5.6 Comparison

Machine learning methods are ideal for fusing because they allow for the use of a variety of inputs [31]. There is a comparison in the Table 2 where all of the machine learning models in dust detection are listed from different researches along with precision, accuracy, AUC, processing time (PT), and RMSE.

The image size in this experiment was  $2030 \times 1053$ . Around 97.5 percent of the 75 million feature vectors were from the context class, with 0.005 percent used for training and the rest for testing. A total of 24 training samples were used per class, with a processing time of 2.5 seconds [48,54,53].

The optimal SVR parameters for 38 dust events with 97 million feature vectors were  $\sigma = 0.125$ ,  $\eta = 0.5$ , and  $\epsilon = 0.1$  [52], where they used 42 million four-dimensional samples with 92 percent precision in this paper [51]. Neural PNN outperforms FFNN, and LP-SVR is the highest, with statistical LP-SVR outperforming ML classifier, which has a false positive rate of more than 50% [49]. They discovered that the output of PNN and LP-SVR is not substantially different when they calculated the crucial difference [49]. TSS assesses all commission and omission mistakes. RF had the highest TSS value, while MARS had the lowest [44].

There are the advantages and disadvantages of using a physical approach over a machine learning approach (55 vs 93 for same day prediction, and 42 vs 80 for different day prediction). The processing time was reduced from 30 hours to 30 minutes thanks to the High Performance Computing Facility (HPCF) [61].

The models' success in predicting the winter dust storm index in Iran's arid regions was addressed [16]. They analyzed Dust Storm Index using MARS,

**Table 2.** Performance Comparison

Model	Ref	Precision	Accuracy	AUC	PT	RMSE
ML	[48,54,53]	0.5255	0.6779	0.4884	0.0141	
PNN	[48,54,53]	0.8080	0.8816	0.7035	0.2393	
FFNN	[48,54,53]	0.7664	0.8412	0.6293	0.0459	
LP-SVR	[48,54,53]	0.7907	0.8678	0.7117	0.0809	
LS LP-SVR	[48,54,53]	0.8295	0.9104	0.7349	0.0974	
PD	[50]	0.3938	0.4964	0.4993	0.0141	
FFNN	[50]	0.4554	0.5426	0.7402	0.0472	
RF	[44,40,62,60]		0.798	0.894		0.16
SVM	[44,40,62,60]		0.658	0.875		0.273
MARS	[44,40]			0.81		0.315
LR	[62,60]		0.839	0.864		
Ensemble	[62,60]		0.756	0.68		

LASSO, k-NN, GP, SVR, Cubist, RF, XGB, DNN, and GRA in the arid area of Iran, and found GRA to be the most accurate where DSI indicates wind erosion.

They measured the efficiency of different machine learning algorithms using AUC and true-skill statistics (TSS). RF was the most successful in deciding that the most critical factors in dust generation were wind speed and land cover [44].

## 6 Other Methods

*Band-math* is a statistical illustration-based method for detecting dust events [48]. Different types of sky can result in different color ratios, which were used to detect dust. Cloud reflectance and emission properties can also be used to observe dust aerosols [61]. They used a neuro-fuzzy inference method that was adaptive (ANFIS). Multivariate and adaptive regression splines were also used (MARS) [44].

Researchers used neural networks and SVM to correct bias between MODIS AOD and AERONET AOD. Since SVM has the property of operating in higher dimensional space with kernel mapping, it outperformed neural networks in bias correction of MODIS Terra and Aqua [29].

## 7 Conclusions

This paper has revised the most common methodologies that are applied to model dust aerosols for different purposes. Dust aerosols can be modeled for detection, probability estimation, discrimination among other aerosols, and even segmentation of dust storms. The general instrument is satellite imagery, which can take different forms depending on the hardware and sensors used to capture atmospheric phenomena. Our study found that the most common sensing type is multispectral, providing a rich spectral signature for different atmospheric analysis tasks.

The most successful algorithms for dust aerosol modeling in earlier work have been based on a straight-forward linear combination of spectral bands. However, with recent advances in machine learning, a lot of work has been successful despite the common explainability critiques. Efficient deep learning models are very good at modeling highly complex phenomena, and it seems like this area requires more exploration. Here are some areas that we identified: i) attention-based recurrent models for exploring dust aerosols over time; ii) convolutional approaches for hyperspectral cubes; and iii) hybrid attention-based deep learning and semi-supervised approaches.

Future work will examine some of these possible areas of experimentation and research the potential advantages of leveraging novel deep learning models.

## References

1. Ackerman, S.A.: Using the radiative temperature difference at 3.7 and 11  $\mu\text{m}$  to tract dust outbreaks. *Remote Sensing of Environment* **27**(2), 129–133 (1989)
2. Ahn, C., Torres, O., Bhartia, P.K.: Comparison of ozone monitoring instrument uv aerosol products with aqua/moderate resolution imaging spectroradiometer and multiangle imaging spectroradiometer observations in 2006. *Journal of Geophysical Research: Atmospheres* **113**(D16) (2008)
3. Aksoy, S., Koperski, K., Tusk, C., Marchisio, G., Tilton, J.C.: Learning bayesian classifiers for scene classification with a visual grammar. *IEEE Transactions on geoscience and remote sensing* **43**(3), 581–589 (2005)
4. Alhichri, H., Alswayed, A.S., Bazi, Y., Ammour, N., Alajlan, N.A.: Classification of remote sensing images using efficientnet-b3 cnn model with attention. *IEEE Access* **9**, 14078–14094 (2021)
5. Alizadeh-Choobari, O., Sturman, A., Zawar-Reza, P.: A global satellite view of the seasonal distribution of mineral dust and its correlation with atmospheric circulation. *Dynamics of atmospheres and oceans* **68**, 20–34 (2014)
6. Badarinath, K., Kharol, S.K., Kaskaoutis, D., Sharma, A.R., Ramaswamy, V., Kambezidis, H.: Long-range transport of dust aerosols over the arabian sea and indian region—a case study using satellite data and ground-based measurements. *Global and Planetary Change* **72**(3), 164–181 (2010)
7. Baddock, M.C., Gill, T.E., Bullard, J.E., Acosta, M.D., Rivera Rivera, N.I.: Geomorphology of the chihuahuan desert based on potential dust emissions. *Journal of Maps* **7**(1), 249–259 (2011)
8. Berndt, E., Elmer, N., Junod, R., Fuell, K., Harkema, S., Burke, A., Feemster, C.: A machine learning approach to objective identification of dust in satellite imagery. *Earth and Space Science* p. e2021EA001788
9. Bishop, J.K., Davis, R.E., Sherman, J.T.: Robotic observations of dust storm enhancement of carbon biomass in the north pacific. *Science* **298**(5594), 817–821 (2002)
10. Boroughani, M., Pourhashemi, S., Hashemi, H., Salehi, M., Amirahmadi, A., Asadi, M.A.Z., Berndtsson, R.: Application of remote sensing techniques and machine learning algorithms in dust source detection and dust source susceptibility mapping. *Ecological Informatics* **56**, 101059 (2020)
11. Butt, M.J., Assiri, M.E., Ali, M.A.: Assessment of aod variability over saudi arabia using modis deep blue products. *Environmental pollution* **231**, 143–153 (2017)

12. Chacon-Murguía, M.I., Quezada-Holguín, Y., Rivas-Perea, P., Cabrera, S.: Dust storm detection using a neural network with uncertainty and ambiguity output analysis. In: Mexican Conference on Pattern Recognition. pp. 305–313. Springer (2011)
13. Chen, J., Huang, H., Peng, J., Zhu, J., Chen, L., Li, W., Sun, B., Li, H.: Convolution neural network architecture learning for remote sensing scene classification. arXiv preprint arXiv:2001.09614 (2020)
14. Chettri, S.R., Crompton, R.F.: Probabilistic neural network architecture for high-speed classification of remotely sensed imagery. *Telematics and Informatics* **10**(3), 187–198 (1993)
15. Dong, R., Xu, D., Jiao, L., Zhao, J., An, J.: A fast deep perception network for remote sensing scene classification. *Remote Sensing* **12**(4), 729 (2020)
16. Ebrahimi-Khusfi, Z., Taghizadeh-Mehrjardi, R., Mirakbari, M.: Evaluation of machine learning models for predicting the temporal variations of dust storm index in arid regions of iran. *Atmospheric Pollution Research* **12**(1), 134–147 (2021)
17. Ekhtesasi, M., Sepehr, A.: Investigation of wind erosion process for estimation, prevention, and control of dss in yazd–ardakan plain. *Environmental monitoring and assessment* **159**(1), 267–280 (2009)
18. Engelstaedter, S., Kohfeld, K., Tegen, I., Harrison, S.: Controls of dust emissions by vegetation and topographic depressions: An evaluation using dust storm frequency data. *Geophysical Research Letters* **30**(6) (2003)
19. Erel, Y., Dayan, U., Rabi, R., Rudich, Y., Stein, M.: Trans boundary transport of pollutants by atmospheric mineral dust. *Environmental science & technology* **40**(9), 2996–3005 (2006)
20. Fjeldsaå, J., Ehrlich, D., Lambin, E., Prins, E.: Are biodiversity ‘hotspots’ correlated with current ecoclimatic stability? a pilot study using the noaa-avhrr remote sensing data. *Biodiversity & Conservation* **6**(3), 401–422 (1997)
21. Hahnenberger, M., Nicoll, K.: Geomorphic and land cover identification of dust sources in the eastern great basin of utah, usa. *Geomorphology* **204**, 657–672 (2014)
22. Huang, J., Fu, Q., Su, J., Tang, Q., Minnis, P., Hu, Y., Yi, Y., Zhao, Q.: Taklimakan dust aerosol radiative heating derived from calipso observations using the fu-liou radiation model with ceres constraints. *Atmospheric Chemistry and Physics* **9**(12), 4011–4021 (2009)
23. Huang, J., Minnis, P., Yi, Y., Tang, Q., Wang, X., Hu, Y., Liu, Z., Ayers, K., Trepte, C., Winker, D.: Summer dust aerosols detected from calipso over the tibetan plateau. *Geophysical Research Letters* **34**(18) (2007)
24. Jiao, P., Wang, J., Chen, X., Ruan, J., Ye, X., Alavi, A.H.: Next-generation remote sensing and prediction of sand and dust storms: State-of-the-art and future trends. *International Journal of Remote Sensing* **42**(14), 5281–5320 (2021)
25. Jin, J., Lin, H.X., Segers, A., Xie, Y., Heemink, A.: Machine learning for observation bias correction with application to dust storm data assimilation. *Atmospheric Chemistry and Physics* **19**(15), 10009–10026 (2019)
26. Kaiser, J.: Mounting evidence indicts fine-particle pollution. *Science* **307**(5717), 1858a–1861a (2005)
27. Kim, S.W., Yoon, S.C., Kim, J., Kim, S.Y.: Seasonal and monthly variations of columnar aerosol optical properties over east asia determined from multi-year modis, lidar, and aeronet sun/sky radiometer measurements. *Atmospheric Environment* **41**(8), 1634–1651 (2007)
28. Kopp, G., Lean, J.L.: A new, lower value of total solar irradiance: Evidence and climate significance. *Geophysical Research Letters* **38**(1) (2011)

29. Lary, D.J., Remer, L., MacNeill, D., Roscoe, B., Paradise, S.: Machine learning and bias correction of modis aerosol optical depth. *IEEE Geoscience and Remote Sensing Letters* **6**(4), 694–698 (2009)
30. Lee, J., Shi, Y.R., Cai, C., Ciren, P., Wang, J., Gangopadhyay, A., Zhang, Z.: Machine learning based algorithms for global dust aerosol detection from satellite images: Inter-comparisons and evaluation. *Remote Sensing* **13**(3), 456 (2021)
31. Li, J., Wong, M.S., Lee, K.H., Nichol, J., Chan, P.: Review of dust storm detection algorithms for multispectral satellite sensors. *Atmospheric Research* p. 105398 (2020)
32. Li, W., Liu, H., Wang, Y., Li, Z., Jia, Y., Gui, G.: Deep learning-based classification methods for remote sensing images in urban built-up areas. *IEEE Access* **7**, 36274–36284 (2019)
33. Liu, J., Chen, B., Huang, J.: Discrimination and validation of clouds and dust aerosol layers over the sahara desert with combined caliop and iir measurements. *Journal of Meteorological Research* **28**(2), 185–198 (2014)
34. Ma, Y., Gong, W.: Evaluating the performance of svm in dust aerosol discrimination and testing its ability in an extended area. *IEEE Journal of Selected Topics in Applied Earth Observations and Remote Sensing* **5**(6), 1849–1858 (2012)
35. Ma, Y., Gong, W., Mao, F.: Transfer learning used to analyze the dynamic evolution of the dust aerosol. *Journal of Quantitative Spectroscopy and Radiative Transfer* **153**, 119–130 (2015)
36. Mahowald, N.M., Bryant, R.G., del Corral, J., Steinberger, L.: Ephemeral lakes and desert dust sources. *Geophysical Research Letters* **30**(2) (2003)
37. Mather, P., Tso, B.: Classification methods for remotely sensed data. CRC press (2016)
38. Mather, P.M., Tso, B., Koch, M.: Geological mapping using multi-sensor data: A comparison of methods. In: *Neurocomputation in Remote Sensing Data Analysis*, pp. 38–46. Springer (1997)
39. Miller, S.: A consolidated technique for enhancing desert dust storms with modis. *Geophysical Research Letters* **30**(20) (2003)
40. Nabavi, S.O., Haimberger, L., Abbasi, R., Samimi, C.: Prediction of aerosol optical depth in west asia using deterministic models and machine learning algorithms.  *Aeolian research* **35**, 69–84 (2018)
41. Namdari, S., Karimi, N., Sorooshian, A., Mohammadi, G., Sehatkashani, S.: Impacts of climate and synoptic fluctuations on dust storm activity over the middle east. *Atmospheric environment* **173**, 265–276 (2018)
42. O’Loingsigh, T., McTainsh, G., Tews, E., Strong, C., Leys, J., Shinkfield, P., Tapper, N.: The dust storm index (dsi): a method for monitoring broadscale wind erosion using meteorological records. *Aeolian Research* **12**, 29–40 (2014)
43. Proietti, A., Panella, M., Leccese, F., Svezia, E.: Dust detection and analysis in museum environment based on pattern recognition. *Measurement* **66**, 62–72 (2015)
44. Rahmati, O., Mohammadi, F., Ghiasi, S.S., Tiefenbacher, J., Moghaddam, D.D., Coulon, F., Nalivan, O.A., Bui, D.T.: Identifying sources of dust aerosol using a new framework based on remote sensing and modelling. *Science of The Total Environment* **737**, 139508 (2020)
45. Ramakrishnan, S., Selvan, S.: Image texture classification using wavelet based curve fitting and probabilistic neural network. *International Journal of Imaging Systems and Technology* **17**(4), 266–275 (2007)
46. Rashki, A., Kaskaoutis, D., Goudie, A., Kahn, R.: Dryness of ephemeral lakes and consequences for dust activity: the case of the hamoun drainage basin, southeastern iran. *Science of the Total Environment* **463**, 552–564 (2013)

47. Rashki, A., Kaskaoutis, D.G., Rautenbach, C.d., Eriksson, P.G., Qiang, M., Gupta, P.: Dust storms and their horizontal dust loading in the sistan region, iran. *Aeolian Research* **5**, 51–62 (2012)
48. Rivas-Perea, P., Rosiles, J., Chacon, M.: Traditional and neural probabilistic multi-spectral image processing for the dust aerosol detection problem. In: 2010 IEEE Southwest Symposium on Image Analysis & Interpretation (SSIAI). pp. 169–172. IEEE (2010)
49. Rivas-Perea, P., Rosiles, J., Cota-Ruiz, J.: Statistical and neural pattern recognition methods for dust aerosol detection. *International journal of remote sensing* **34**(21), 7648–7670 (2013)
50. Rivas-Perea, P., Rosiles, J., Tilton, J.: Dust storm detection trough moderate resolution imaging spectroradiometer: A machine learning problem
51. Rivas-Perea, P., Cota-Ruiz, J.: Nert dads: A near-real-time dust aerosol detection system
52. Rivas-Perea, P., Rivas-Perea, P.E., Cota-Ruiz, J., Aragon Franco, R.: Near real-time dust aerosol detection with support vector machines for regression. In: AGU Fall Meeting Abstracts. vol. 2015, pp. A23C–0331 (2015)
53. Rivas-Perea, P., Rosiles, J.G.: A probabilistic model for stratospheric soil-independent dust aerosol detection. In: *Digital Image Processing and Analysis*. p. DMD4. Optical Society of America (2010)
54. Rivas-Perea, P., Rosiles, J.G., Murguia, M.I.C., Tilton, J.J.: Automatic dust storm detection based on supervised classification of multispectral data. In: *Soft Computing for Recognition Based on Biometrics*, pp. 443–454. Springer (2010)
55. Rivera Rivera, N.I.: Detection and characterization of dust source areas in the chihuahuan desert, southwestern north america (2006)
56. Ruckstuhl, C., Norris, J.R.: How do aerosol histories affect solar “dimming” and “brightening” over europe?: Ipccl-ar4 models versus observations. *Journal of Geophysical Research: Atmospheres* **114**(D10) (2009)
57. Shahrisvand, M., Akhoondzadeh, M.: A comparison of empirical and intelligent methods for dust detection using modis satellite data. *International Archives of the Photogrammetry, Remote Sensing and Spatial Information Sciences* **1**(W3), 371–375 (2013)
58. Shao, Y., Wang, J.: A climatology of northeast asian dust events. *Meteorologische Zeitschrift* **12**(4), 187–196 (2003)
59. Shawky, O.A., Hagag, A., El-Dahshan, E.S.A., Ismail, M.A.: Remote sensing image scene classification using cnn-mlp with data augmentation. *Optik* **221**, 165356 (2020)
60. Shi, L., Zhang, J., Zhang, D., Igbawua, T., Liu, Y.: Developing a dust storm detection method combining support vector machine and satellite data in typical dust regions of asia. *Advances in Space Research* **65**(4), 1263–1278 (2020)
61. Shi, P., Song, Q., Patwardhan, J., Zhang, Z., Wang, J.: Mineral dust detection using satellite data. UMBC Physics Department (2020)
62. Shi, P., Song, Q., Patwardhan, J., Zhang, Z., Wang, J., Gangopadhyay, A.: A hybrid algorithm for mineral dust detection using satellite data. In: 2019 15th International Conference on eScience (eScience). pp. 39–46. IEEE (2019)
63. Someya, Y., Imasu, R., Shiomi, K.: Dust aerosol detection by the modified co2 slicing method. *Sensors* **19**(7), 1615 (2019)
64. Song, J., Gao, S., Zhu, Y., Ma, C.: A survey of remote sensing image classification based on cnns. *Big earth data* **3**(3), 232–254 (2019)



65. Souri, A.H., Vajedian, S.: Dust storm detection using random forests and physical-based approaches over the middle east. *Journal of Earth System Science* **124**(5), 1127–1141 (2015)
66. Specht, D.F.: Probabilistic neural networks for classification, mapping, or associative memory. In: ICNN. pp. 525–532 (1988)
67. Vickery, K.J., Eckardt, F.D.: Dust emission controls on the lower kuiseb river valley, central namib. *Aeolian Research* **10**, 125–133 (2013)
68. Walker, A.L., Liu, M., Miller, S.D., Richardson, K.A., Westphal, D.L.: Development of a dust source database for mesoscale forecasting in southwest asia. *Journal of Geophysical Research: Atmospheres* **114**(D18) (2009)
69. Wang, Q., Liu, S., Chanussot, J., Li, X.: Scene classification with recurrent attention of vhr remote sensing images. *IEEE Transactions on Geoscience and Remote Sensing* **57**(2), 1155–1167 (2018)
70. Wei, K., Zhang, T., He, B.: Detection of sand and dust storms from meris image using fe-otsu alogrithm. In: 2008 2nd international conference on bioinformatics and biomedical engineering. pp. 3852–3855. IEEE (2008)
71. Xie, Y.: Detection of smoke and dust aerosols using multi-sensor satellite remote sensing measurements. Ph.D. thesis (2009)
72. Zhang, L., Zhou, W., Jiao, L.: Wavelet support vector machine. *IEEE Transactions on Systems, Man, and Cybernetics, Part B (Cybernetics)* **34**(1), 34–39 (2004)
73. Zhang, W., Tang, P., Zhao, L.: Remote sensing image scene classification using cnn-capsnet. *Remote Sensing* **11**(5), 494 (2019)
74. Zhao, T.X.P., Ackerman, S., Guo, W.: Dust and smoke detection for multi-channel imagers. *Remote Sensing* **2**(10), 2347–2368 (2010)